Chapter 3 Modeling, Simulation, and Optimized Design of Micro-machined inductor

3.1 Introduction

In this chapter, we will drive the model of proposed micro-machined inductor. The modeling target is expected that designer can get significant information from this model as accurately as commercial electromagnetic simulator, but the cost time will be diminished greatly. Moreover, we also can accomplish the optimized scale of structure of micro-machined inductor using this model. As known, the RF spiral inductors have been developed for a long time and their characteristics, including inductance, capacitance, loss mechanism, etc., have been surveyed in detail. There are many methodologies to calculate those parameters, such as Greenhouse's formula [7] and physics-based closed-form expression [8] for inductance, and distributed capacitance model (DCM) [9] for capacitance value. Therefore, we can synthesize those methodologies to develop an exactly equivalent model for the micro-machined inductor. By the model, designer could integrate the high-Q micro-machined inductor with their circuit to enhance the performance and reduce noise effect. Finally, the simulated and measured results of devices will be in contrast with the droved model.

Before starting on the modeling, some geometric parameters of spiral inductor must be defined conscientiously. The geometry of the planar spiral inductor without bridge connector can be specified by the following parameters: number of turns, **n**, the width of metal, **w**, spacing between adjacent turns, **s**, the thickness of metal, **t**, the inner diameter, **din**, and the outer diameter, **dout**, as shown in Figure 3-1 [13].

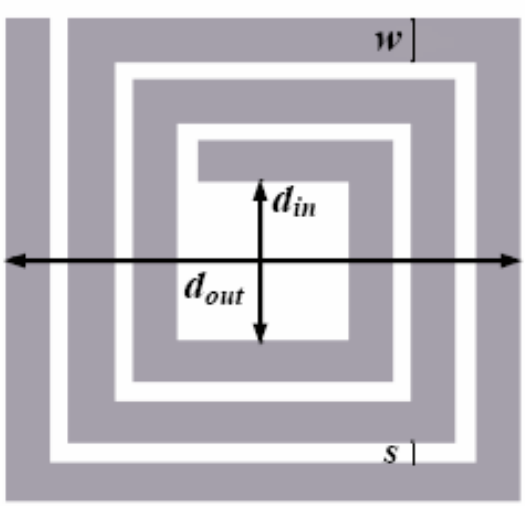

Fig. 3-1 A square spiral inductor with three turns [12].

As mentioned in the section 2.2.2, the equivalent circuit model of the micro-machined inductor with silicon substrate removal can be simplified as figure 3-2. As long as the three components can be accurately analyzed using electromagnetic analysis, the behavior of spiral inductor will be predicted. With appropriate approximations, we can get an accurate and computationally efficient approach to determinate the value of *Cs*, *Ls*, and *Rs*. In the next sections, we will focus on the evaluation of *Cs*, *Ls*, and *Rs*.

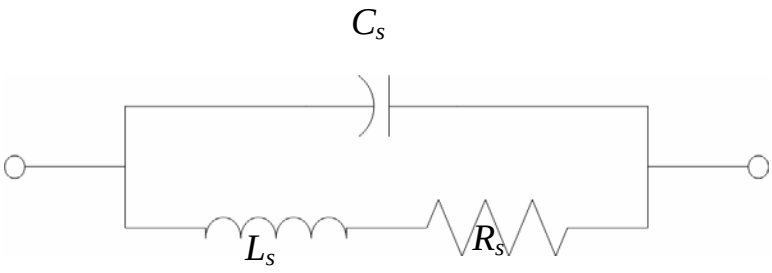

Fig.3-2 The equivalent circuit model of micro-machined inductor with the substrate removal.

3.2 Inductance Calculation

According Greenhouse's theory [7], the inductance of planar square spiral inductor can be calculated analytically with appropriate approximations. Based on Greenhouse's conception, the total inductance of an inductor is split up into sections consisting of the inductor self-inductance (L_{self}), the mutual inductance (L_M), and the contribution of other components. Meanwhile, the mutual inductance comes from tow parts including the total positive mutual (L_{M+}) and the total negative mutual inductances (L_{M-}). Recently, a proposed physics-based closed-form inductance expression will be a useful methodology for inductance calculation. In contrast with Greenhouse's algorithm, the summing one by one individual segment interactions, the physics-based closed-form inductance expression was based on the average segment interaction. Otherwise, this expression can easily define a spiral inductor with "half-turn" turns for another conspicuous advantage. Due to its physics-based nature, the expression also is scalable in geometry [8].

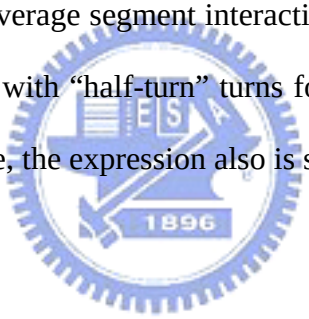

3.2.1 Self-inductance

At first, the planar square spiral inductor can be decomposed into segments, as shown figure 3-3. It is convenient to calculate by defining **din'** as

$$d_{in}' = d_{in} + (w + s) \tag{3.1}$$

where **din** is the inner diameter. In the figure 3-3, the length of the segments increases with steps (w + s), and the increase occurs every two segments. Then the total length of the inductor l is

$$l = d_{in}'(4n+1) + N_i(4N_i+1)\cdot(w+s) \tag{3.2}$$

where Ni is the integer part of **n**. Hence, there are averagely n segments on every four sides of inductor. That is, the length of an average segment $l_{seg\,avg}$ is

$$l_{seg\ avg} = \frac{l}{4n} \tag{3.3}$$

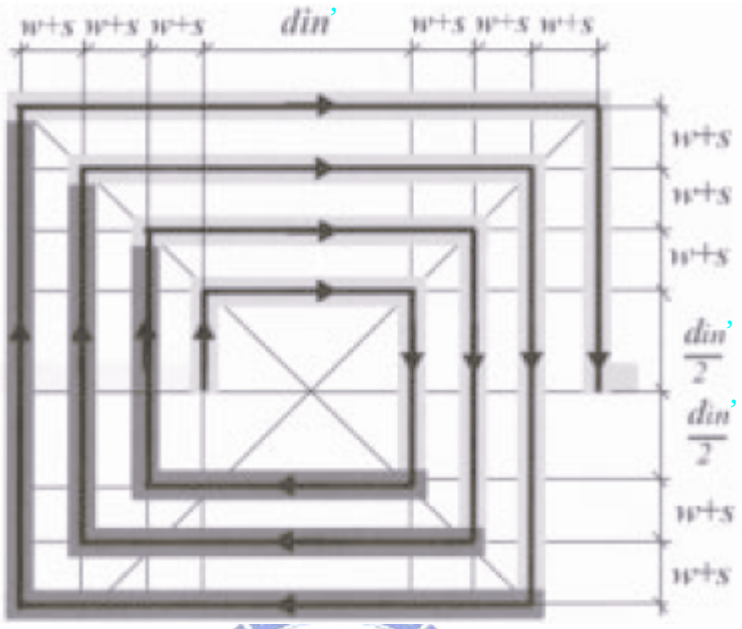

Fig.3-3 An inductor with n = 3.5 turns is decomposed into segments [7].

For a straight line with the length *lseg*, the self-inductance can be shown as [7]

$$L_{self} = \frac{\mu}{2\pi} l_{seg} \left(\ln\left(\frac{2 \cdot l_{seg}}{GMD}\right) - 1.25 + \frac{AMD}{l_{seg}} + \frac{u}{4} \cdot T \right) \tag{3.4}$$

where μ is the permeability of conductor. GMD and AMD represent the geometric and arithmetic mean distance, respectively. T is the frequency-correction parameter. When the conductor has the rectangular dimension of cross section, the self-inductance at radio frequency can be driven as

$$L_{self} = \frac{\mu}{2\pi} l_{seg} \left(\ln\left(\frac{2 \cdot l_{seg}}{w+t}\right) + 0.50049 + \frac{w+t}{3 \cdot l_{seg}} \right) \tag{3.5}$$

where *w* and *s* are the width and thickness, respectively. There are totally 4*n* segments

with the average length *lseg avg* in a square spiral inductor. That is, the total self-inductance is the sum of self-inductance of 4*n* segments. According to equation (3.3) and (3.5), the total self-inductance of spiral square inductor can be expressed as

$$L_{self\ total} = 4n \cdot \left[\frac{\mu}{2\pi} \cdot \frac{l}{4n} \left(\ln\left(\frac{2 \cdot \frac{l}{4n}}{w+t} \right) + 0.50049 + \frac{w+t}{3 \cdot \frac{l}{4n}} \right) \right]$$

thus,

$$L_{self\ total} = \frac{\mu}{2\pi} l \left(\ln\left(\frac{l}{n \cdot (w+t)} \right) - 0.2 + \frac{4n \cdot (w+t)}{3 \cdot l} \right) \tag{3.6}$$

3.2.2 Mutual Inductance

Let's consider the layout in the following figure 3-4,

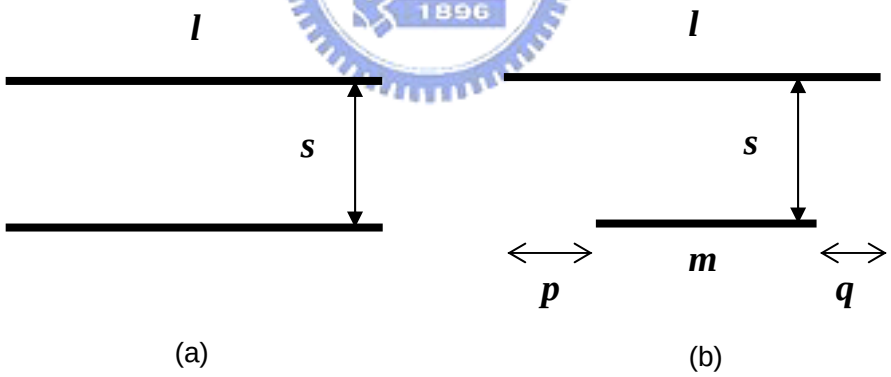

Fig. 3-4 Two parallel-filament geometry (a) with equal length, and (b) with different length.

the mutual inductance of figure 3-4 (a) can be derived as [7]

$$L_M = \frac{\mu}{2\pi} \cdot l \left[\ln\left(\frac{l}{s} + \sqrt{1 + \left(\frac{l}{s} \right)^2} \right) - \sqrt{1 + \left(\frac{l}{s} \right)^2} + \frac{s}{l} \right] \tag{3.7}$$

Moreover, the general formula for the mutual inductance of the given filaments can be found to be the result of combining the mutual inductances of four pairs of equal parallel filaments. For example, Using equation 3.7, the mutual inductance of a structure shown in figure 3-4 (b) is presented analytically as

$$L_M = \frac{1}{2} \cdot \left[(M_{m+p} + M_{m+q}) - (M_p + M_q) \right] \tag{3.8}$$

where M_x means the mutual inductance of two parallel tracks with equal length *x*.

As mentioned previously, the contribution of mutual inductance will be separated two parts: the total positive mutual (L_{M+}) and the total negative inductances (L_{M-}). It is distinguished according to the direction of current flowing in the conductor. The anti-direction currents in the both segments will contribute the negative mutual inductance. Otherwise, the parallel segments will contribute the positive inductance. Figure 3-5 (a) shows the section of figure 3-3, that Segments on the opposite sides of the square spiral inductor contribute to the negative mutual inductance. Due the symmetry property of square inductor, the sum of interactions that contribute negative inductance can be approximated as $2n^2$ average interactions. On the other hand, there are $2n^2$ interactions of negative inductance produced between segments of an average length at an average distance. For the structure in figure 3-5 (a), it is a coincidence that the average distance d^- between segments of a square spiral inductor is equal to the average segment length $l_{seg\ avg}$. Consequently, utilizing the equation (3.8), the total negative inductance can be presented as a simple function of the total length *l* and the number of turns *n* as

$$L_{M-} = 2 \cdot 2n^2 \left\{ \frac{\mu}{2\pi} \cdot l_{seg\,avg} \left[\ln\left(\frac{l_{seg\,avg}}{d^-} + \sqrt{1 + \left(\frac{l_{seg\,avg}}{d^-} \right)^2} \right) - \sqrt{1 + \left(\frac{l_{seg\,avg}}{d^-} \right)^2} + \frac{d^-}{l_{seg\,avg}} \right] \right\}$$

Using equation (3.3) and $d^{-} = l_{seg\ avg}$, thus

$$L_{M-} = 2 \cdot 2n^2 \cdot \left(\frac{\mu}{2\pi} \cdot \frac{l}{4n} \cdot \left[\ln\left(1+\sqrt{2}\right) + 1 - \sqrt{2} \right] \right) \cong \frac{\mu}{2\pi} \cdot l \cdot n \cdot 0.47 \tag{3.9}$$

The mechanism of interactions of positive inductance is shown in the figure 3-5 (b). Those parallel segments on the same side of a square inductor will make positive effect to mutual inductance. In the same way, the average distance d^{+} for the constituting factor of positive mutual inductance can be driven by a closed form as

$$d^{+} = (w+s) \cdot (N_i + 1) \cdot \frac{3n - 2_i - 1}{3 \cdot (2n - N_i - 1)} \tag{3.10}$$

Thus, the total positive inductance is

$$L_{M+} = \frac{\mu}{2\pi} \cdot l \cdot (n-1) \left\{ \ln \left[\sqrt{1 + \left(\frac{l}{4nd^{+}} \right)^2} + \frac{l}{4nd^{+}} \right] - \sqrt{1 + \left(\frac{l}{4nd^{+}} \right)^2} + \frac{4nd^{+}}{l} \right\} \tag{3.11}$$

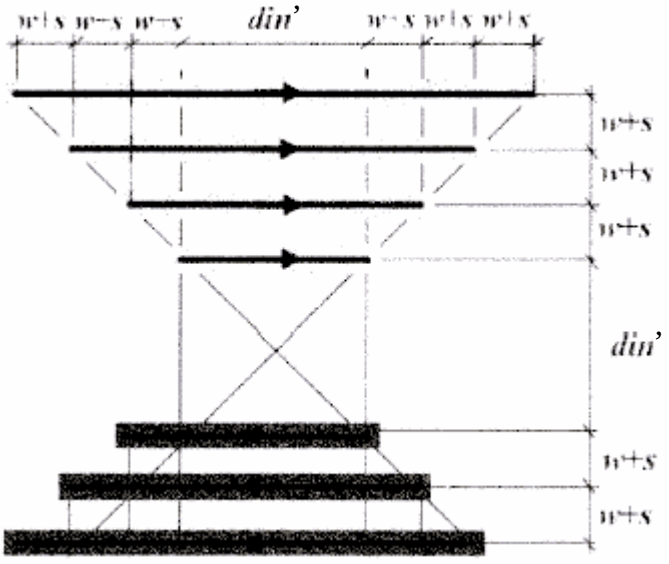

(a)

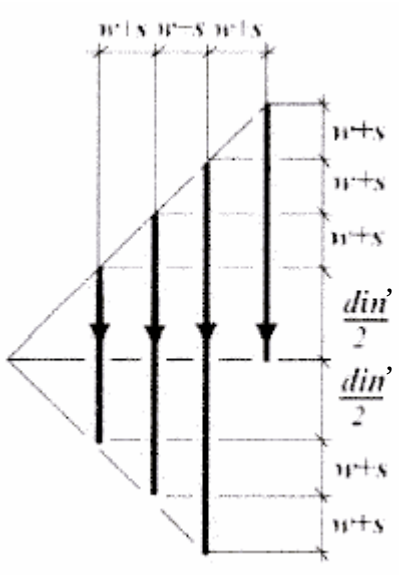

(b)

Fig. 3-5 (a) Segments on the opposite sides of the square spiral inductor contribute to the negative mutual inductance. (b) Segments on the same sides of the square spiral inductor contribute to the positive mutual inductance [7].

3.2.3 Other Contribution

The contribution of principal part of square spiral inductor has been discussed above paragraphs. Actually, except main coil, the micro-machined inductor must include the connector such as the bridge. Figure 3-6 shows the layout of square planar spiral inductor. The bridge's effect for inductance must be considered, especially for the inductor of small inductance. In general, the bridge is located at the center of geometry of rectangular inductor. Moreover, the effect of mutual inductance between the bridge and the metal track perpendicular to the bridge can almost be neglected. Otherwise, due to the counteraction on induced effect between the bridge and the metal track parallel to it, the contribution of mutual inductance of the bridge can be taken for the interaction between the bridge and the closest parallel metal track, as shown in figure 3-6 (a). In the same way, we can use the driven equation (3.6) and (3-11) to calculate the

self-inductance and mutual inductance yielded by the bridge [14]. The total inductive effect of the bridge is denoted as L_{bridge}.

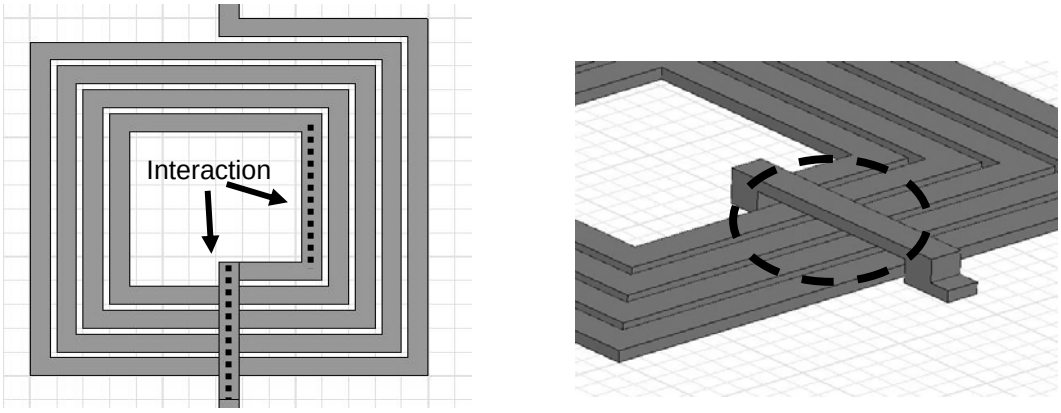

(a) (b)

Fig. 3-6 (a)The layout of square planar spiral inductor, (b) the oblique view.

So,

$$L_{self\ \ bridge} = \frac{\mu}{2\pi} l_{bridge}\left(\ln\left(\frac{l_{bridge}}{n\cdot(w+t)}\right) - 0.2 + \frac{4n\cdot(w+t)}{3\cdot l_{bridge}}\right)$$

$$L_{m+} = \frac{\mu}{2\pi}\left[\begin{array}{l}\alpha\sinh^{-1}\frac{2\alpha}{din} - l_{bridge}\sinh^{-1}\frac{2l_{bridge}}{din} - 1.44\cdot din + \\ -\sqrt{\alpha^2+din^2} + \sqrt{{l_{bridge}}^2+din^2} + (\sqrt{2}-1)\cdot din\end{array}\right]$$

$$\alpha = l_{bridge} + din$$

$$L_{bridge} = L_{self\ \ bridge} + L_{m+}$$

Finally, the total inductance L_s of square planar spiral inductor can be expressed from equation (3.6), equation (3-11) and L_{bridge} as

$$L_s = L_{self\ total} + \left(L_{M+} - L_{M-}\right) + L_{bridge} \qquad (3.12)$$

and,

$$L_s = \frac{\mu}{2\pi} \cdot l \cdot \left\{ \begin{array}{l} \ln\left[\frac{l}{n\cdot(w+t)}\right] - 0.2 - 0.47\cdot n + \\ (n+1)\cdot\left(\ln\left[\sqrt{1+\left(\frac{l}{4nd^+}\right)^2} + \frac{l}{4nd^+}\right] - \sqrt{1+\left(\frac{l}{4nd^+}\right)^2} + \frac{4nd^+}{l} \right) \end{array} \right\} + L_{bridge} \quad (3.13)$$

It should be noted that parameters in equation (3.13) are just the geometry parameters of the inductor, and there are also no unphysical fitting factor. It is clearly a physics-based closed-form expression. Besides, it can show circuit designer what the relative contributions of self-inductance, positive, negative mutual inductance, and the bridge based on the geometry parameters are.

3.3 Capacitance Calculation

3.3.1 Distributed Capacitance Model

At the higher operating frequency, the parasitic capacitive effect of inductors will make important influences to electrical performance. Moreover, The distributed capacitance models (DCMs) for spiral inductors have been developed to accurately estimate the equivalent capacitive coupling capacitance C_s between and the two terminals and the equivalent parasitic capacitance between the metal strips and the underneath substrate C_{si}, as shown in figure 2-4 of the chapter 2 .

The fundamental assumptions of DCM are based on the conception that the voltage distributes over the spiral inductor, as called voltage profile [9][15]. In the viewpoint of energy, DCM will derive the total stored energy electrically with the voltage profile of a inductor and extract the equivalent capacitance value overall the inductor. In the

following section, we will evaluate the capacitance C_s using DCM. The starting point of the derivation of capacitance formula is that some reasonable assumptions will be declared for simplicity. First, the width of metal track of inductor *w* is much larger than the spacing between the adjacent tracks *s*. On the other hand, we will neglect the spacing to calculate the inductor's area and total length in the process of the derivation of capacitance formula. Secondly, voltage distribution is proportional to the length of the metal tracks. It means that the longer the metal track is, the larger the voltage drop on the track is. Third, the voltage is regarded as constant value in the same, and the value is determined by the averaging the beginning voltage and the ending voltage of the turn.

3.3.2 The Evaluation of Capacitance C_s

Figure 3-7 presents the voltage profile and DCM of the n-turn on-chip spiral inductor, where the outermost turn is numbered as first turn and the innermost turn is numbered as nth turn. $C_{mm}(n-1,n)$ shows the equivalent capacitance between the *(n-1)*th and *n*th turn. And $C_{ms}(n)$ is the equivalent parasitic capacitance between the metal strip of *n*th turn and the underneath substrate. As mentioned previously, the substrate of micro-machined inductor has been removed to reducing substrate losses so that the effect of substrate can be ignored. Therefore, C_{si} is regard as zero, i.e., $C_{ms}(n)$ is neglected. In this brief, we will focus on the calculation of C_s for the micro-machined inductor at radio frequencies.

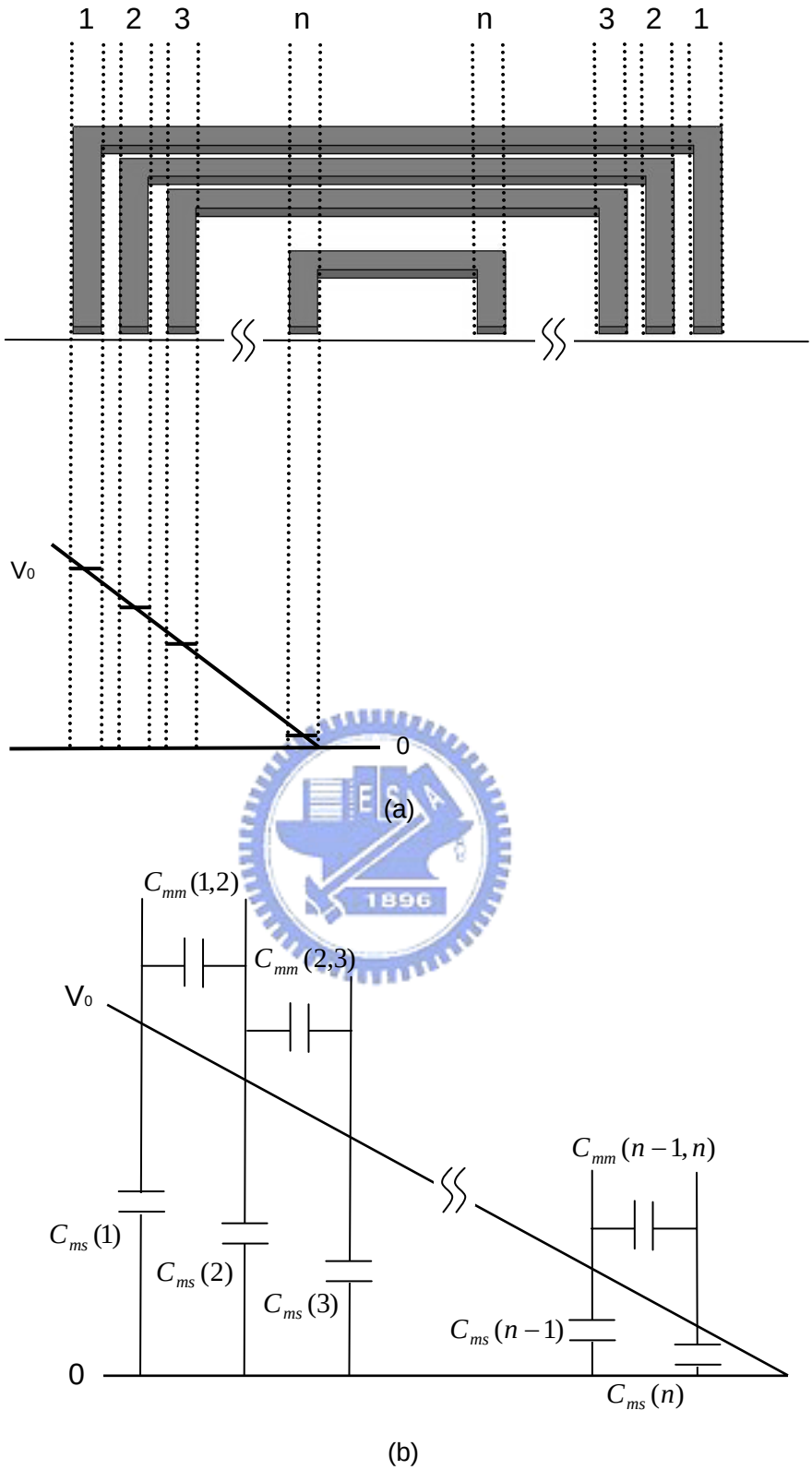

Fig. 3-7 (a)The voltage profile of a planar spiral inductor. (b) Distributed capacitance model of the n-turn on-chip planar spiral inductor [8].

First, the lengths of each turn can be defined as l_1, l_2, l_3, …., l_n, so that the total

length *l* is

$$l = l_1 + l_2 + l_3 + \Lambda + l_n \tag{3.14}$$

As shown in figure 3-7, V_0 is the applied voltage across the micro-machined inductor. Moreover, the beginning voltage $V(k)_{begin}$ and the ending voltage $V(k)_{end}$ of the *k*th turn can be derived as

$$V(k)_{begin} = V_0\left[1-\left(h_1 + h_2 + \Lambda + h_{k+1}\right)\right] \tag{3.15}$$

$$V(k)_{end} = V_0\left[1-\left(h_1 + h_2 + \Lambda + h_{k+1} + k_k\right)\right] \tag{3.16}$$

where

$$h_k \equiv \frac{l_k}{l}$$

Based on the third assumption made previously, the voltage of the *k*th turn can be expressed as

$$V(k) = \frac{1}{2}\left[V(k)_{begin} + V(K)_{end}\right]$$

thus,

$$\begin{aligned} V(k) &= \frac{1}{2}\cdot V_0 \cdot \left[1-\left(h_1 + h_2 + \Lambda + h_{k+1}\right) + 1 - \left(h_1 + h_2 + \Lambda + h_{k+1} + k_k\right)\right] \\ &= \frac{1}{2}\cdot V_0 \cdot \left[2 - d(k-1) - d(k)\right] \end{aligned} \tag{3.17}$$

where

$$d(k) = h_1 + h_2 + \Lambda + h_k$$

Then the voltage difference between the *k*th and *(k+1)*th turn of micro-machined inductor can be shown as

$$\begin{aligned} \Delta V(k, k+1) &= V(k) - V(k+1) \\ &= \frac{1}{2}\cdot V_0 \cdot \left[d(k+1) - d(k-1)\right] \end{aligned} \tag{3.18}$$

Using equation (3.18), the electrical energy stored in the capacitor between the *k*th and

*(k+1)*th turn of micro-machined inductor is

$$E_{mm}(k) = \frac{1}{2} \cdot C_{mm} \cdot l_k \cdot \Delta V(k, k+1)^2 \tag{3.19}$$

where C_{mm} is the capacitance per unit length between adjacent metal tracks. For the rectangular dimension of cross section of two conductors with the width w_1 and w_2, C_{mm} can be expressed analytically as a closed-form formula [16]

$$C_{mm} = \frac{2\pi\varepsilon_{r(eff)}\varepsilon_0}{\ln\left[\pi^2 \cdot \left[\frac{w_1 + w_2}{2} + s\right]^2 \cdot \left(\frac{1}{w_1 + t}\right) \cdot \left(\frac{1}{w_2 + t}\right)\right]} \quad F/m \tag{3.20}$$

where $\varepsilon_{r(eff)}$ is the effective dielectric constant accounts for non-homogeneity of the region surrounding conductors. *s* and *t* are the spacing and thickness of conductor, respectively. When w_1 is equal to w_2, the expression can be rewrote as

$$C_{mm} = \frac{\pi\varepsilon_{r(eff)}\varepsilon_0}{\ln\left(\frac{\pi(s+w)}{w+t} + 1\right)} \quad F/m \tag{3.21}$$

Thus, the total electrical energy stored in the metal-to-metal capacitor of micro-machined inductor can be expressed as

$$\begin{aligned} E_{total} &= \sum_{k=1}^{n-1} E_{mm}(k) \\ &= \frac{1}{8} \cdot \sum_{k=1}^{n-1} C_{mm} \cdot l_k \cdot \left[d(k+1) - d(k-1)\right]^2 \\ &= \frac{1}{2} \cdot C_s \cdot V_0^2 \end{aligned} \tag{3.22}$$

thus, the equivalent capacitive coupling capacitance between and the two terminals *Cs* is

$$C_s = \frac{1}{4} \cdot \sum_{k=1}^{n-1} C_{mm} \cdot l_k \cdot \left[d(k+1) - d(k-1) \right]^2 \qquad (3.23)$$

3.4 Series Impedance Calculation

As mentioned in the section 2.2.1.1, the series impedance R_s resulted from conductor is interrelated to the skin effect. In general, the series impedance R_s of conductor can be expressed as [17]

$$R_s = \frac{l}{w \cdot \sigma \cdot \delta \cdot \left(1 - \exp\left(\frac{-t}{\delta} \right) \right)} \quad \text{(Ohms)} \qquad (3.24)$$

where δ is the skin depth. σ is the conductivity of metal. *l*, *w*, and *t* represent the overall length, width, and thickness of conductor strip, respectively. It should be noted that R_s is the function of skin depth δ, and δ is the function of frequency. Thus, the series impedance will increase with the increasing of the operating frequency.

3.5 Simulated Method

Although the driven model is useful to help us to design a micro-machined inductor, it is still essential to verify the model utilizing the computational simulator. In this thesis, the contemporary 3-D electromagnetic simulated soft, Ansoft HFSS (version 9.2), was adopted to analyze electromagnetically the characteristics of micro-machined inductor. The Simulator HFSS was installed on a personal computer with CPU of Intel Pentium(R) 4 2.4 GHz and DDR ram 1G. Ansoft HFSS has the advantages that it could simulate the non-planar structures, such as micro-machined inductors, using the finite element method (FEM). But that will consequentially cost lots of time to obtain a reasonable

solution. The micro-machined inductor with cross membrane was put in air surrounded by boundary condition (BC), i.e. radiation, except the two waveports. Figure 3-8 (a) shows the simulated environment in HFSS that the two waveports and the boundary condition are made for the micro-machined inductor. In general, it is difficult and important to construct the setup of the port-source and boundary condition of simulated object. In experience, to get the approach solution with limited computer resource, the distance between BC and the center of inductor was set up as twelve times of inductor's scale. In addition, the ground-signal-ground (GSG) pads, such as a coplanar waveguide without lower ground plane, were attached to the terminals of inductor as measured pads, as shown in figure 3-8 (b). The scale of two square waveports is about eight times of the width of signal pad ***h*** [18]. After simulation, the effect of GSG pads will be de-embedded on the S-parameter. The results of modeling, simulation, and measurement will be summarized in the chapter 5.

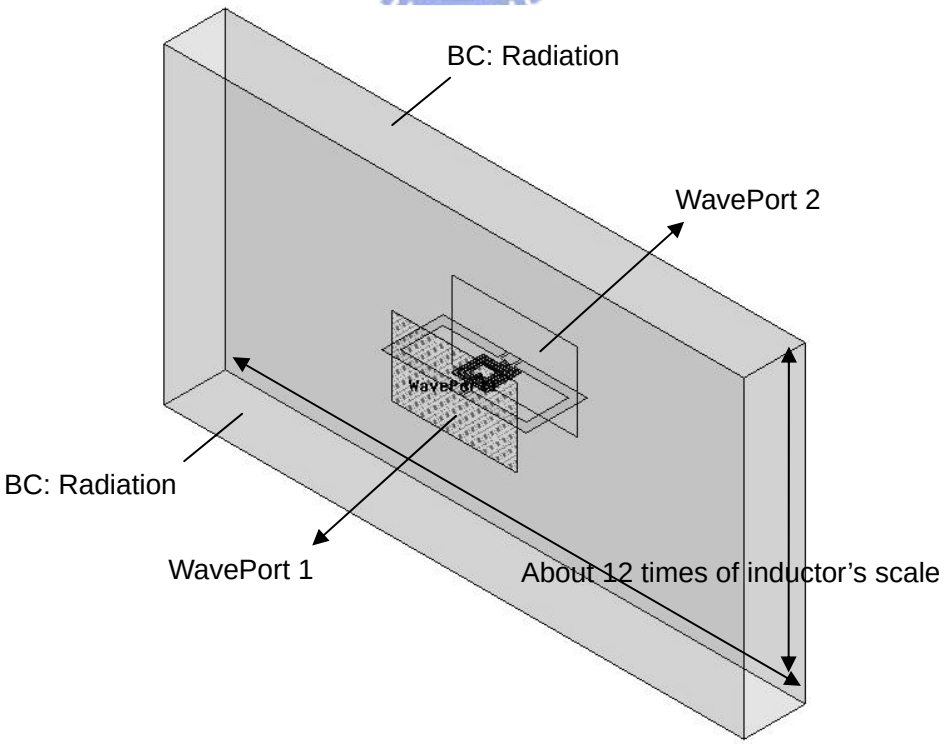

(a)

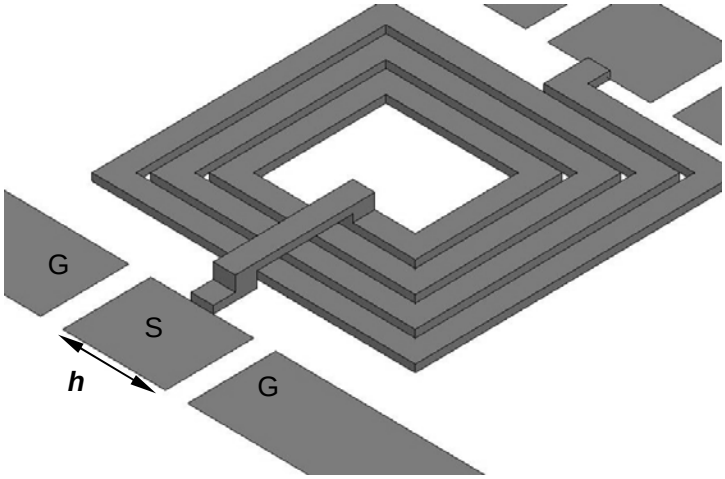

(b)

Fig. 3-8 (a) The simulated environment, (b) Ground-signal-ground (GSG) pads are connected to the micro-machined inductor.

3.6 Optimized design

Now we can utilize driven model to achieve the optimized design of micro-machined inductor. The target of optimized design is to have the lowest cost (or area), diminish the effect of parasitic capacitance, and gain higher Q value with inductance 0.5 nH ~ 5 nH at the frequencies 1 GHz ~ 10 GHz. According to physics-based closed-form inductance model, the parameters **din** and **n** obviously have more effectively inductance than the others. Therefore, first we will decide the most adaptive values **of s**, **w**, and **t**. For this reason, the expected inductance could be obtained by tuning the **din** and **n** values.

Because the skin depth of copper is about 2.1 um at frequency 1 GHz, the thickness of metal tracks **t** must be higher than 4.2 um (∵ two sides). Moreover, parameter **t** is sensitive to parasitic capacitance apparently. For this reason, we tradeoff the **t** value to 5 um. For **s** value**,** thinking of lower cost and the limit of photolithography process, it is decided that **s** is 5 um; for **w** value, in order to gain higher quality factor value, **w** is

better to be larger. However, due to the fixed thickness, the Q value will saturate with the increasing **w**. At last, w was fixed on 15 um. By the sake of realizing the micro-machined inductor with cross membrane, the center of inductor must be reserved for spacing. There is a minimum limitation to **din**, and that is $d_{in} \geq 30um$. As we know from above, the design rule about the scale of micro-machined inductor could be summarized as table 2. One will gain a specified inductance from the corresponding number of turn and inner diameter, as shown figure 3-9.

Frequencies: 1GHz ~ 10GHz

t = 5 um ; s = 5 um ; w = 15 um					
n	1.5	2.5	3.5	4.5	5.5
L (nH)	~ 0.8	0.8 ~ 1.8	1.7 ~ 2.9	2.9 ~ 4.7	4.7 ~

Table 3-1 The rule of Optimized design for micro-machined RF spiral inductor.

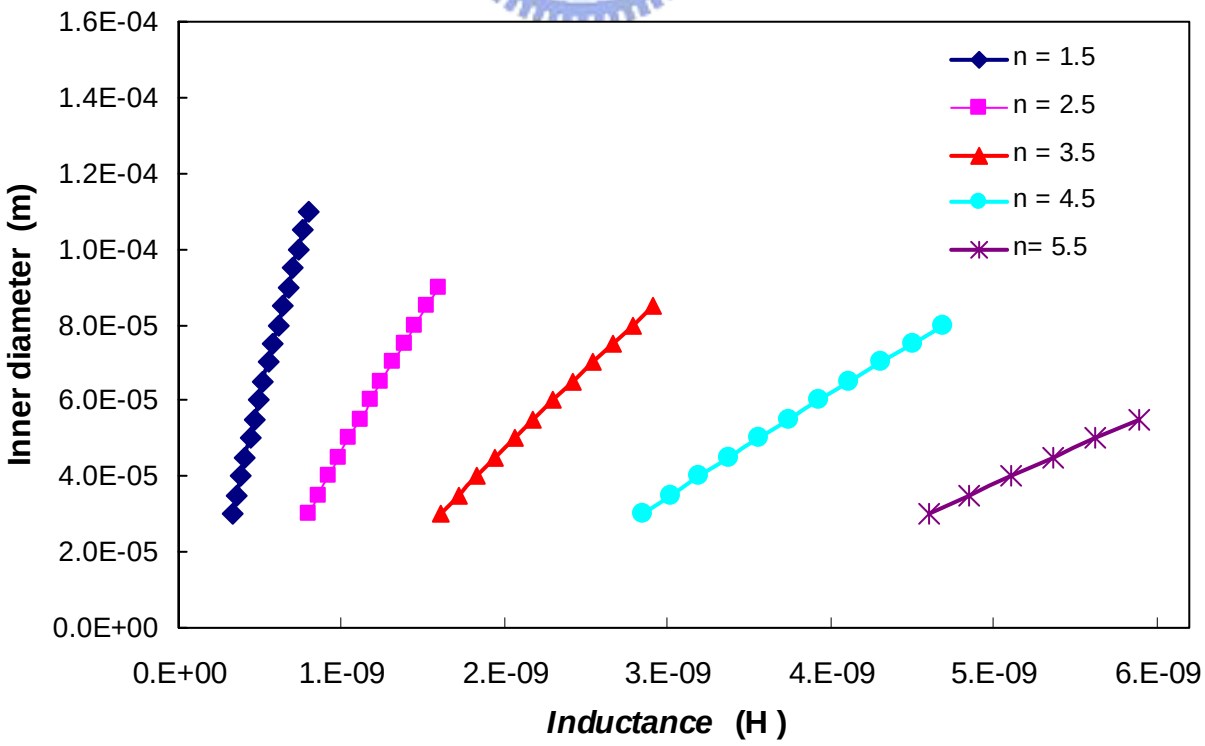

Fig. 3-9 The rule of Optimized design for micro-machined RF spiral inductor.